Gypsum-Dependent Effect of NaCl on Strength Enhancement of CaO-Activated Slag Binders

Sungwon Sim [1], Hwan Lee [1], Dongho Jeon [1], Haemin Song [1], Woo Sung Yum [1], Dohoon Kim [1], Jung-Il Suh [1,2] and Jae Eun Oh [1,*]

[1] School of Urban and Environmental Engineering, Ulsan National Institute of Science and Technology (UNIST), UNIST-gil 50, Ulju-gun, Ulsan 44919, Korea; simsung@unist.ac.kr (S.S.); hwanindeayo@unist.ac.kr (H.L.); jeondongho@unist.ac.kr (D.J.); haemin93@unist.ac.kr (H.S.); reikoku@unist.ac.kr (W.S.Y.); elvis03@unist.ac.kr (D.K.); rgtonesuh@snu.ac.kr (J.-I.S.)
[2] Department of Architecture and Architectural Engineering, Seoul National University, 1, Gwanak-ro, Gwanak-Gu, Seoul 08826, Korea
* Correspondence: ohjaeeun@unist.ac.kr

check for updates

Abstract: This study explores the combined effect of NaCl and gypsum on the strength of the CaO-activated ground-granulated blast furnace slag (GGBFS) binder system. In the CaO-activated GGBFS system, the incorporation of NaCl without gypsum did not improve the strength of the system. However, with the presence of gypsum, the use of NaCl yielded significantly greater strength than the use of either gypsum or NaCl alone. The presence of NaCl largely increases the solubility of gypsum in a solution, leading to a higher concentration of sulfate ions, which is essential for generating more and faster formations of ettringite in a fresh mixture of paste. The significant strength enhancement of gypsum was likely due to the accelerated and increased formation of ettringite, accompanied by more efficient filling of pores in the system.

Keywords: CaO-activation; slag; gypsum; NaCl; cementless binder; construction binder

1. Introduction

Ground-granulated blast furnace slag (GGBFS) is an industrial waste byproduct generated in the steel manufacturing industry. Extensive investigations have examined the use of GGBFS as a construction material to replace Portland cement for concrete production; in particular, numerous studies have focused on utilizing GGBFS as a precursor material in producing cementless binders [1–8].

Sodium-based alkaline activators (e.g., NaOH, Na-silicate) have been widely used to activate the binding properties of GGBFS to produce strong cementless binders for construction purposes (e.g., alkali-activated slag) [5,9,10]; however, because these activators are significantly more expensive than Portland cement, alkali-activated GGBFS binders are not commonly used in construction sites. Furthermore, alkaline activators are not safe for workers due to their high pH levels (>14) resulting in high toxicity [11].

Recently, calcium-based activators (e.g., $Ca(OH)_2$, CaO) have been reported for their use of activating GGBFS because these activators are less expensive and have less alkaline than sodium-based activators [6,11–13]. In the manufacturing process of commercial GGBFS, sulfate sources (e.g., gypsum ($CaSO_4 \cdot 2H_2O$), anhydrite ($CaSO_4$)) are often incorporated to improve grinding efficiency and satisfy the required national standards of chemical composition for industrial uses [14]. When gypsum is present, CaO activation produces significantly higher strength when activating GGBFS, mainly due to the formation of ettringite ($Ca_6Al_2(SO_4)_3(OH)_{12} \cdot 26H_2O$) [12]; Thus, the solubility of gypsum is an important factor in increasing the strength of the CaO-activated GGBFS system.

The use of sodium chloride (NaCl) in cementless binder systems may also affect strength development; For instance, Bellman et al. [1], reported that the addition of NaCl notably increased the compressive strength of activated GGBFS with calcium hydroxide ($Ca(OH)_2$) and calcium carbonate ($CaCO_3$). Further, in alkali-activated GGBFS, the addition of NaCl changed strength development and setting time, which is defined as the measured amount of time it takes for a freshly mixed paste to solidify [10].

Most previous studies have looked at chlorides and sulfates as aggressive environmental agents, focusing primarily on the durability issues of cementitious materials (e.g., chloride binding capacity, embedded steel corrosion, or sulfate attack) [15–23] rather than their effects as additives.

Thus, this study investigated the influences of adding NaCl to the CaO-activated GGBFS system on strength development and the dependence of strength enhancement effect on the presence of gypsum in the system. However, the significance of chloride-induced corrosion is not specifically considered because this study was a preliminary study to develop cementless binders for manufacturing blocks or bricks, which do not contain any steel.
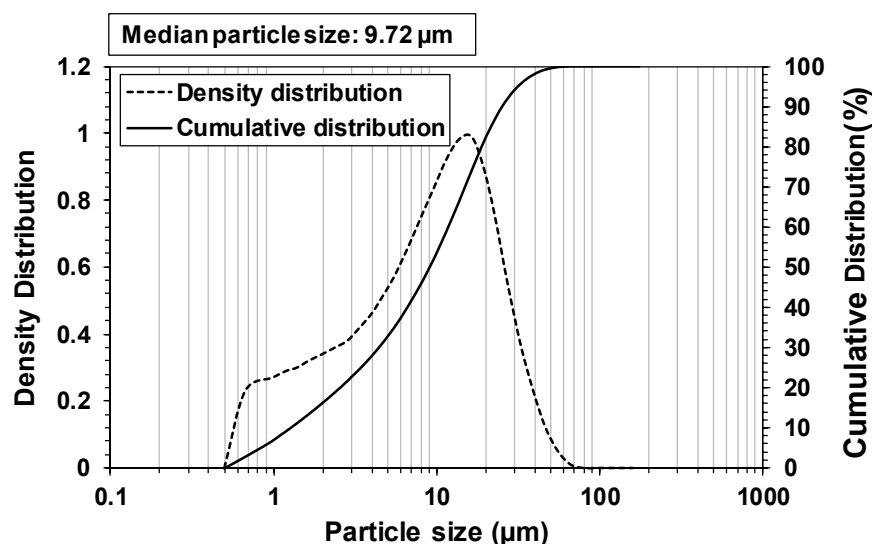
To this end, compressive strength testing, powder X-ray diffraction (XRD), thermogravimetry (TG), and mercury intrusion porosimetry (MIP) were conducted.

2. Materials and Methods

A commercial GGBFS with no gypsum was purchased in the Republic of Korea. The chemical composition of the GGBFS is presented in Table 1, and was obtained using X-ray florescence (XRF). The particle size distributions of the GGBFS were measured using a laser diffraction particle size analyzer (HELOS (HI199), and RODOS, Sympatec, Clausthal-Zellerfeld, Germany), as shown in Figure 1.

Table 1. Chemical composition of ground-granulated blast furnace slag (GGBFS) (wt %).

Formula	CaO	SiO_2	Al_2O_3	MgO	SO_3	TiO_2	K_2O	Fe_2O_3	Na_2O	MnO
Oxide content	44.3	34.3	14.3	3.3	1.4	0.7	0.6	0.5	0.3	0.3

Figure 1. Particle size distribution of ground-granulated blast furnace slag (GGBFS).

The mixture proportions of paste samples are shown in Table 2. The following chemicals used in this study were of analytical grades: CaO (Daejung Chemicals, Siheung, Korea), NaCL (Duksan Chemicals, Ansan, Korea), and gypsum ($CaSO_4 \cdot 2H_2O$, Sigma Aldrich, St. Louis, MO, US). CaO was used as the main activator for the GGBFS to achieve a binding property, while NaCl and gypsum were

incorporated as replacements for the GGBFS. The water-to-binder weight ratio (wt %/wt %) was set at 0.35 for all mixture samples.

Table 2. Mixture proportions of paste samples (wt %).

Sample Label	Binder				Water
	GGBFS	CaO	NaCl	Gypsum	
Ca-N0-G0 (Control)	95	5	0	0	35
Ca-N0-G5	90	5	0	5	35
Ca-N1-G0	94	5	1	0	35
Ca-N1-G5	89	5	1	5	35

The solubilities of gypsum and $Ca(OH)_2$, which is a hydrated form of CaO, are 15.13 and 19.76 mmol/kg·H_2O, respectively, in pure water at 25 °C; when 1 g of NaCl is present in 35 g of water at 25 °C, the solubilities of gypsum and $Ca(OH)_2$ increase to 15.13–39.44 and 27.18–29.11 mmol/kg·H_2O, respectively [24,25]. Thus, as in this study, the addition of NaCl is likely to make gypsum and CaO more soluble.

All binder components (GGBFS, CaO, NaCl, and gypsum) were dry-mixed and then mixed further with water. For compressive strength testing, ASTM C 109 [26] requires the use of two or three identical samples; however, in this study, six identical paste samples were prepared for each proportion of the mixture using $5 \times 5 \times 5$ cm cubic molds to ensure the reliability of the strength testing results. For MIP testing, the pastes were cast in cylindrical samples (ϕ 2.54 $\times$ 2.54 cm). All cast paste samples were cured in a humidity chamber at 23 °C with a relative humidity above 99% for all curing periods. For the TG and XRD tests, fractured samples were collected after compressive strength tests and finely ground. The MIP test may cause significant deviations from actual pore structures due to microstructural damage by non-wetting liquid (i.e., mercury) [27], and/or the ink-bottle effect [28]. However, despite the drawbacks, the MIP test is still widely accepted for evaluating microstructural changes of hardened cementitious pastes due to compositional changes, similar to those in this study, when samples are prepared with proper sizes and drying conditions are satisfied [29–31]. For the MIP test, cylindrical samples were cut into cubic samples with dimensions of $5 \times 5 \times 5$ mm. All prepared samples were immersed in isopropanol for 24 h to prevent any further reaction and then dried out in a vacuum desiccator before instrumental testing.

To consider the effect of (1) NaCl content, (2) gypsum content, and (3) gypsum–NaCl interaction on strength, *p*-values were calculated through the F-test of the analysis of variance (ANOVA) [32]. Note that the *p*-value is a significance level of the null hypothesis. First, it is assumed that a chosen factor is not influential. When a calculated *p*-value for the chosen factor is lower than 0.05, the null hypothesis is considered false at a 95% confidence level.

Powder XRD patterns for raw GGBFS and hardened samples were collected using a high-power X-ray diffractometer (D/MAX 2500V/PC, Rigaku, Tokyo, Japan) with Cu-Kα radiation (λ = 1.5418 Å) from 5° to 60° in 2θ degree intervals. The XRD patterns were analyzed using the International Center for Diffraction Data (ICDD) PDF-2 database [33] and the Inorganic Crystal Structure Database (ICSD) [34]. TG data were measured using a simultaneous thermal analyzer (SDT Q600, TA Instruments, New Castle, DE, USA), beginning at room temperature and increasing to 1000 °C at a heating rate of 10 °C/min in a N_2 condition using an alumina pan. For more precise analysis, the XRD and TG tests were performed for two identical samples of each sample mixture.

Pore size distributions for the hardened samples were estimated using a mercury porosimeter (Autopore IV, Micrometrics, Atlanta, GA, USA).

3. Results and Discussion

3.1. Compressive Strength

The compressive strength test results of all hardened paste samples are provided in Figure 2. Each strength result shows an averaged value obtained from six identical samples.

A previous study [12], reported that the use of gypsum significantly increased the strength of CaO-activated GGBFS. Similarly, in this study, the 5 wt % of gypsum incorporation (Ca-N0-G5 in Table 2) significantly increased the strength, which is consistent with the previous study.

When NaCl was used without gypsum (Ca-N1-G0), when compared to the mixture without NaCl or gypsum (Ca-N0-G0), no strength improvement was achieved at 7 days, and the strength was even lower at 28 days. However, the sample with both NaCl and gypsum (Ca-N1-G5) demonstrated noticeably higher strength results than Ca-N0-G5 at 7 and 28 days. This shows that the use of NaCl was only beneficial in improving strength when paired with gypsum in this study.

It is worth noting that the beneficial effect of NaCl combined with gypsum on strength seems to have mostly occurred before 7 days. This is evidenced by the fact that most of the strength gains of Ca-N0-G5 and Ca-N1-G5 were obtained before 7 days.
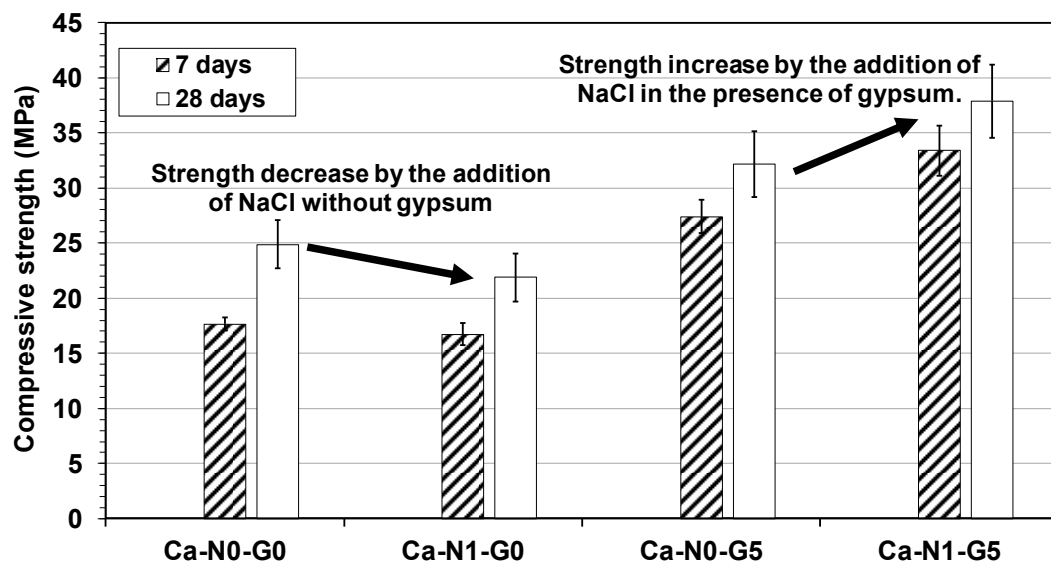

Figure 2. Compressive strengths of hardened paste samples. The error bars indicate standard deviations.
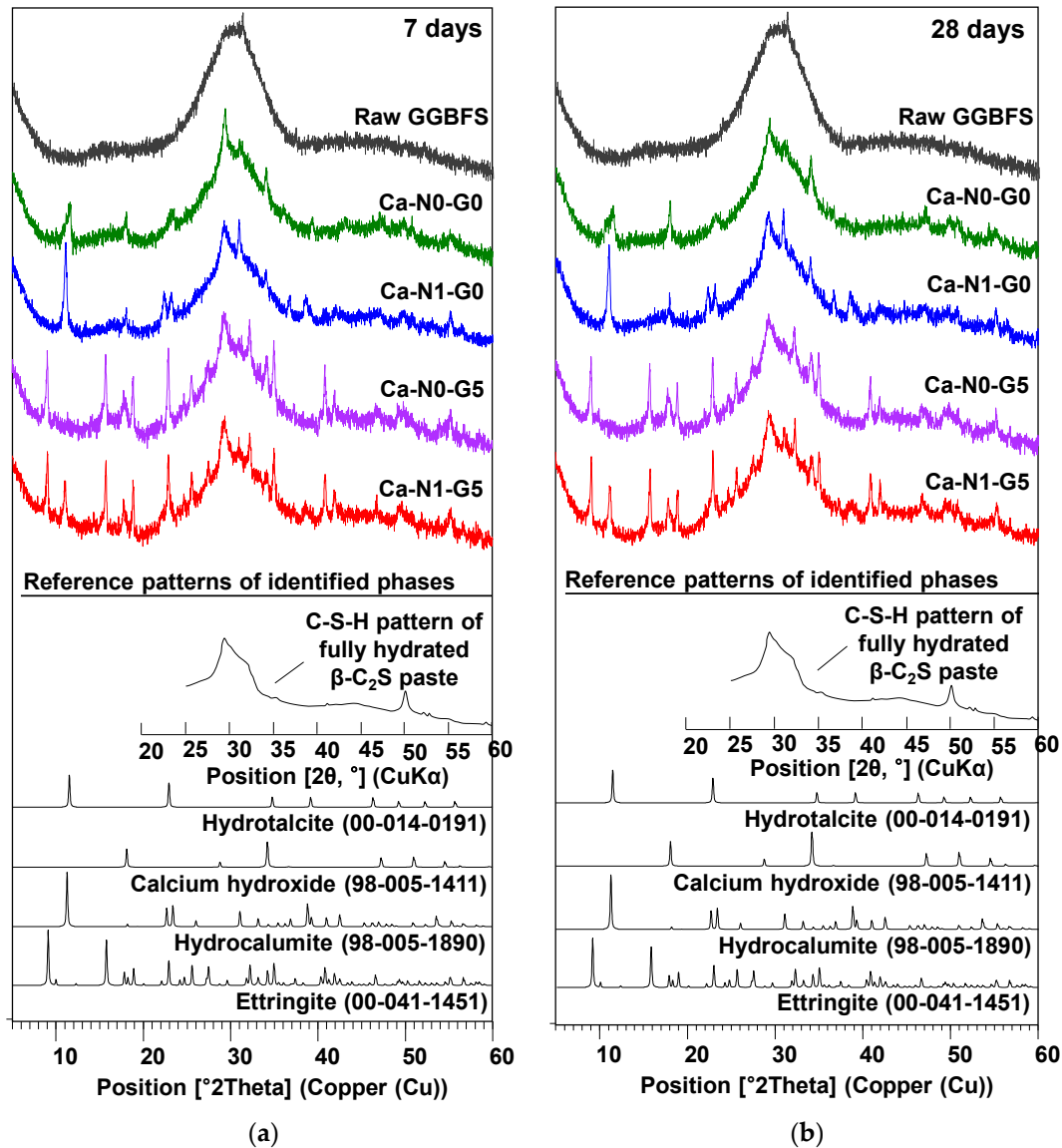
3.2. ANOVA Analysis

The *p*-value for each factor (i.e., NaCl content, gypsum content, and gypsum–NaCl interaction) was calculated by the F-test of the ANOVA as shown in Table 3. The *p*-values of the gypsum content and the gypsum–NaCl interaction were smaller than 0.05 at all days, implying that these factors were significantly influential on strength at all days. However, the *p*-value of the NaCl content became larger than 0.05 at 28 days, unlike at 7 days, which indicates that the influence of the NaCl content on strength was significant at 7 days, but was largely decreased at 28 days.

Table 3. *p*-values for the compressive strengths of hardened paste samples.

Factor	*p*-Value	
	7 Days	28 Days
NaCl content	0.000461	0.2349
Gypsum content	<0.00001	<0.00001
Gypsum–NaCl interaction	0.00014	0.00082

3.3. Powder X-Ray Diffraction (XRD)

The XRD patterns of hardened samples are presented in Figure 3, along with the reference patterns of identified phases. Table 4 shows the list of reaction products generated in each sample.

Figure 3. X-ray diffraction (XRD) patterns of hardened pastes at (**a**) 7 and (**b**) 28 days. Note that the reference XRD pattern for calcium silicate hydrate (C-S-H) was taken from a 22-year-old β-C_2S paste from an earlier study after removing the peaks of $Ca(OH)_2$ [35]. The numbers in parentheses indicate the International Center for Diffraction Data (ICDD) and Inorganic Crystal Structure Database (ICSD) reference numbers for the identified phases.

Table 4. Identified reaction products of hardened paste samples (O: Formation, X: No formation).

Sample Label	Reaction Products				
	C-S-H	Hydrotalcite	$Ca(OH)_2$	Ettringite	Hydrocalumite
Ca-N0-G0 (Control)	O	O	O	X	X
Ca-N1-G0	O	X	O	X	O
Ca-N0-G5	O	X	O	O	X
Ca-N1-G5	O	X	O	O	O

All hardened samples produced calcium silicate hydrate (C-S-H) and calcium hydroxide ($Ca(OH)_2$).

In the sample that did not have NaCl or gypsum (Ca-N0-G0), weak peaks of hydrotalcite ($Mg_6Al_2CO_3(OH)_{16}\cdot4H_2O$) were identified. Hydrotalcite has often been found in alkali- or CaO-activated GGBFS pastes and in blends of Portland cement with GGBFS [2,6,12,13,36]. Hydrotalcite belongs to layered double hydroxides (LDHs), which consist of a family of minerals with the general formula of $[M^{II}_{1-x}M^{III}_x(OH)_2]^{x+}[A^{n-}_{x/n}]^{x-}\cdot yH_2O$, where A^{n-} = n-valent anion, M^{II} = divalent cations, and M^{III} = trivalent cations, and they are closely related to brucite ($Mg(OH)_2$) in their basic structure.

When NaCl and/or gypsum were incorporated in this study, hydrotalcite was mostly removed, and the use of NaCl (Ca-N1-G0) yielded hydrocalumite (($Ca_2Al(OH)_6(Cl_{1-x}(OH)_x)\cdot3(H_2O)$, x = 0–1, Al_2O_3-Fe_2O_3-mono (AFm) [7], phase)), while the incorporation of gypsum (Ca-N0-G5) produced ettringite ($Ca_6Al_2(SO_4)_3(OH)_{12}\cdot26H_2O$), which is known as a strength enhancing material by filling pores [12,37]. These reaction products have often been observed in earlier studies of construction binders containing chloride [13,38–40] or sulfate sources [12,41,42].

The use of $CaCl_2$ has been reported to produce hydrocalumite and result in strength improvement of fly ash and lime-slag blend binders due to pore size refinement [3,40,43]. Although the use of NaCl in this study also generated hydrocalumite, it was not effective in increasing strength when added without gypsum.

When NaCl and gypsum were present together (Ca-N1-G5), hydrocalumite and ettringite were simultaneously formed. However, no other types of new reaction products were identified, contrary to the results of cases with only NaCl or gypsum added. Previous studies have reported that hydrotalcite has a significant capacity for chloride binding [36,44–46] and ion-exchange for SO_4^{2-} [47], indicating that the removal of hydrotalcite was likely due to the presence of NaCl and/or gypsum in the corresponding samples.
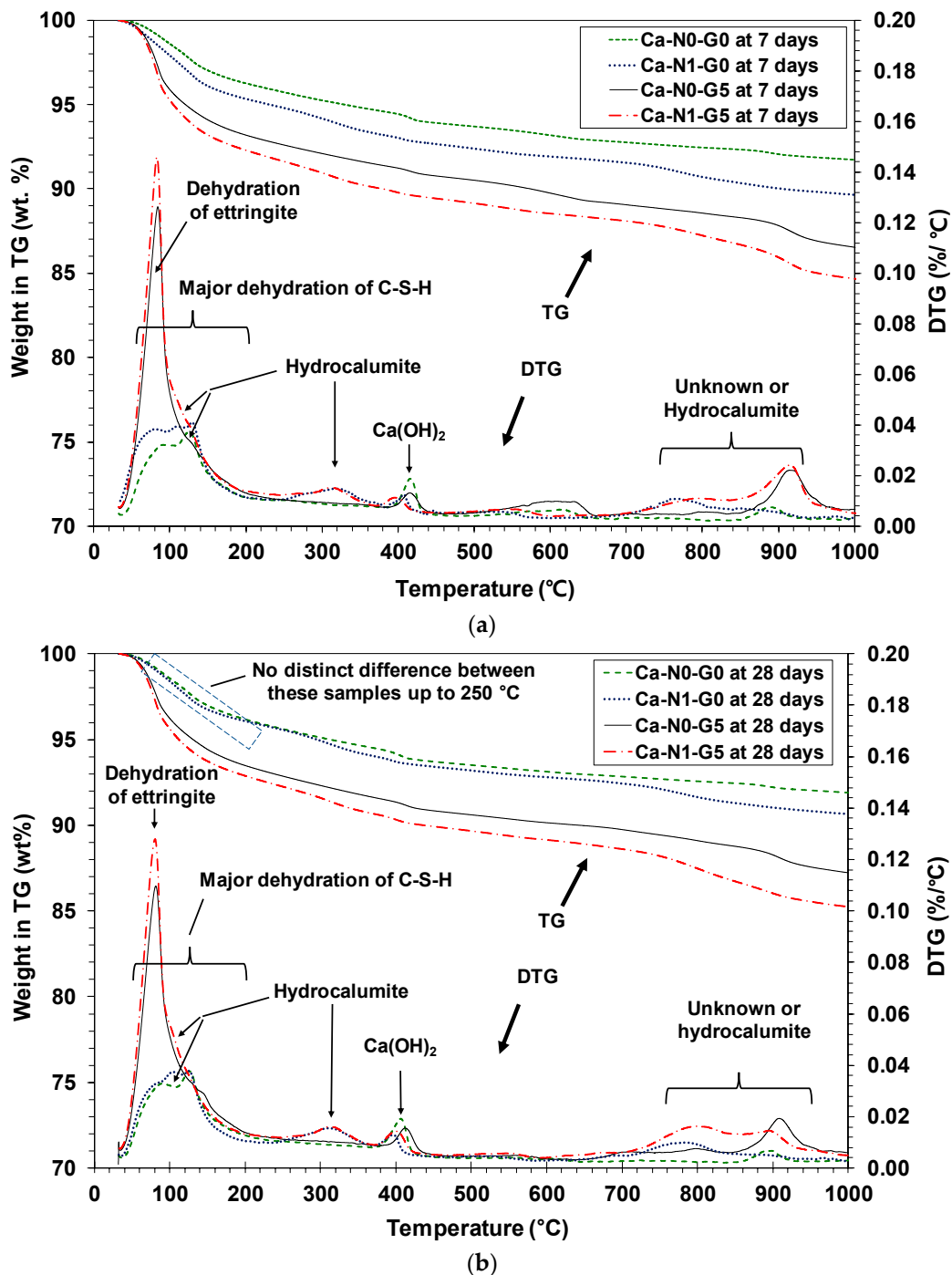
3.4. Thermogravimetric (TG) Analysis

The TG plots and their differential thermogravimetry (DTG) curves are shown with the identified decomposed phases in Figure 4. In this study, the results of XRD and TG tests showed complexity and inconsistency at all days as follows: (1) The XRD peaks of hydrocalumite in Ca-N1-G0 were much greater than those in Ca-N1-G5, while their DTG peaks were very similar at around 250–400 °C; (2) the XRD peaks of ettringite exhibited similar intensities in Ca-N0-G5 and Ca-N1-G5, while the DTG peak of ettringite near 80 °C in Ca-N0-G5 was smaller than that of Ca-N1-G5. These discrepancies were confirmed, as the XRD and TG were measured twice for two identical samples of each mixture at all days.

In addition, when comparing the results of the DTG of TG plots between 7 and 28 days, the weight losses at 7 days were generally higher than those at 28 days. This is abnormal, because as the curing process progresses more weight accumulates for reaction products, which are generally thermally decomposable. However, as stated earlier, the TG/DTG was conducted for duplicate samples of each mixture at each day of curing, and their results showed consistency between duplicate samples, indicating that this discrepancy in the TG/DTG data between 7 and 28 days was more likely due to a change in the sample preparation process between these days that went unnoticed. For instance, ettringite is highly sensitive to any change in drying conditions during preparation [48–50]. Nonetheless, as the detecting resolution of XRD appeared relatively lower than TG in this study, the analysis of TG/DTG was mainly used to examine reaction product quantities for each day of curing and the results showed adequate consistency between the samples with the same curing days.

The results of phase identification in DTG were fairly consistent with the results of XRD at each day of curing. Dehydration of C-S-H [51,52] and ettringite [7,52,53] were identified at 0–200 °C in DTG. Song et al. [53] reported that ettringite was completely removed at 60 °C and the dehydration of C-S-H started from 100 °C in the $Ca(OH)_2$-activated GGBFS system, which is a similar binder system

to that of this study. Thus, although the decomposition temperature ranges of ettringite and C-S-H were closely spaced, they are sufficiently distinguishable for reliable interpretation.

Figure 4. Thermogravimetry (TG) and differential thermogravimetry (DTG) results of hardened samples at (**a**) 7 and (**b**) 28 days.

The decomposition of hydrocalumite was identified in the following three temperature ranges: 25–250 °C, 250–400 °C, and around 800 °C [40,54]. Dehydration of $Ca(OH)_2$ [53,55], was identified at 400–450 °C.

In the samples with NaCl and/or gypsum, several weight losses were observed, overlapped with the weight loss of hydrocalumite near 800 °C, in the range of 600–900 °C. Given that no other

crystalline phase besides ettringite or hydrocalumite was identified in the XRD analysis of these samples, these additional weight losses were likely related to unknown types of amorphous phases.

In the 30–140 °C range in the TG test, when NaCl was used with gypsum, the use of NaCl (Ca-N1-G5) observably increased the weight loss of ettringite when compared to that of the sample with only gypsum (Ca-N0-G5) at all curing days. In general, ettringite mostly forms and contributes to strength within three days of curing in cementitious binders with sulfate sources [8,12,37,56]. The presence of NaCl also increases the solubility of gypsum [24]. Thus, Figure 2 shows that because the most strength improvement using NaCl with gypsum was obtained before 7 days, the use of NaCl likely boosted the formation of ettringite by notably increasing the concentrations of calcium and sulfate ions in the early days (i.e., before three days), which resulted in improving early strengths.

In addition, when comparing the weight losses of $Ca(OH)_2$ for Ca-N0-G0 and Ca-N1-G0 at around 430 °C, the use of NaCl clearly reduced the weight loss of $Ca(OH)_2$ at all days. Note that the presence of NaCl in the pore solution generally increases the solubility of $Ca(OH)_2$ [57]. Thus, $Ca(OH)_2$ in Ca-N1-G0 tended to exist in an ionic state and was used to form Ca-bearing reaction products; for instance, in Figure 4a, Ca-N1-G0 showed more dehydration of C-S-H than Ca-N0-G0; although, this difference nearly disappeared at 28 days. It is noteworthy that despite forming more C-S-H, the strength of Ca-N1-G0 was not higher than that of Ca-N0-G0, which will be discussed further in Section 3.5.

3.5. Mercury Intrusion Porosimetry (MIP)

The pore size distributions of hardened paste samples at 7 and 28 days are presented in Figure 5. In hardened cementitious pastes, pores ranging from 0.01 to 1 μm are known as capillary pores, and they are significantly detrimental to strength due to their angular pore shapes.

Larger sizes of capillary pores generally result in reduced strength, while strength tends to increase as total porosity decreases, pore size distribution is more influential than the total porosity [7,8,58–60]. Given these conditions, the MIP results of this study elaborate on the compressive strength testing results provided in Figure 2.

Park et al. [12], reported that the strength of CaO-activated slag was significantly improved by adding gypsum mainly due to the effect of pore size refinement through substantial ettringite formation, and the use of 10% gypsum achieved the greatest compressive strength. Similar result was obtained in the Ca-N0-G5 samples of this study.

When no gypsum was present, at 7 days, the total porosity of Ca-N1-G0 was slightly smaller than that of Ca-N0-G0, which is consistent with the observation that more C-S-H formed in Ca-N1-G0 than in Ca-N0-G0 at 7 days, as shown in the TG/DTG results. However, the use of NaCl did not beneficially affect the pore size distribution for increasing strength at 7 days because, as shown in the gray highlighted shades for Ca-N1-G0 in Figure 5a. Although relatively small pores were reduced, larger sizes of pores increased when compared to that of Ca-N0-G0. At 28 days, while Ca-N1-G0 still contained a large portion of original big pores (ranging from 0.02 to 0.04 μm), the use of NaCl hindered the refinement of pore sizes, which consists of the process of reducing total porosity and overall pore size. Meanwhile, Ca-N1-G0 also experienced slight reduction of total porosity from 7 to 28 days. These observations are fairly consistent with their corresponding strength results.

When gypsum was present, the influence of NaCl showed a substantially positive influence on pore size distribution. Although the average pore sizes of Ca-N0-G5 and Ca-N1-G5 were similar at 7 days, relatively large pores (indicated by the diagonal line pattern of Ca-N0-G5 in Figure 5a) were removed in Ca-N1-G5 after adding NaCl in the presence of gypsum, exhibiting the greatest strength of Ca-N1-G5 among all samples at 7 days.

At 28 days, although the difference in pore size distribution mostly disappeared between Ca-N0-G5 and Ca-N1-G5, the Ca-N1-G5 still showed slightly smaller overall pore sizes than that of Ca-N0-G5.
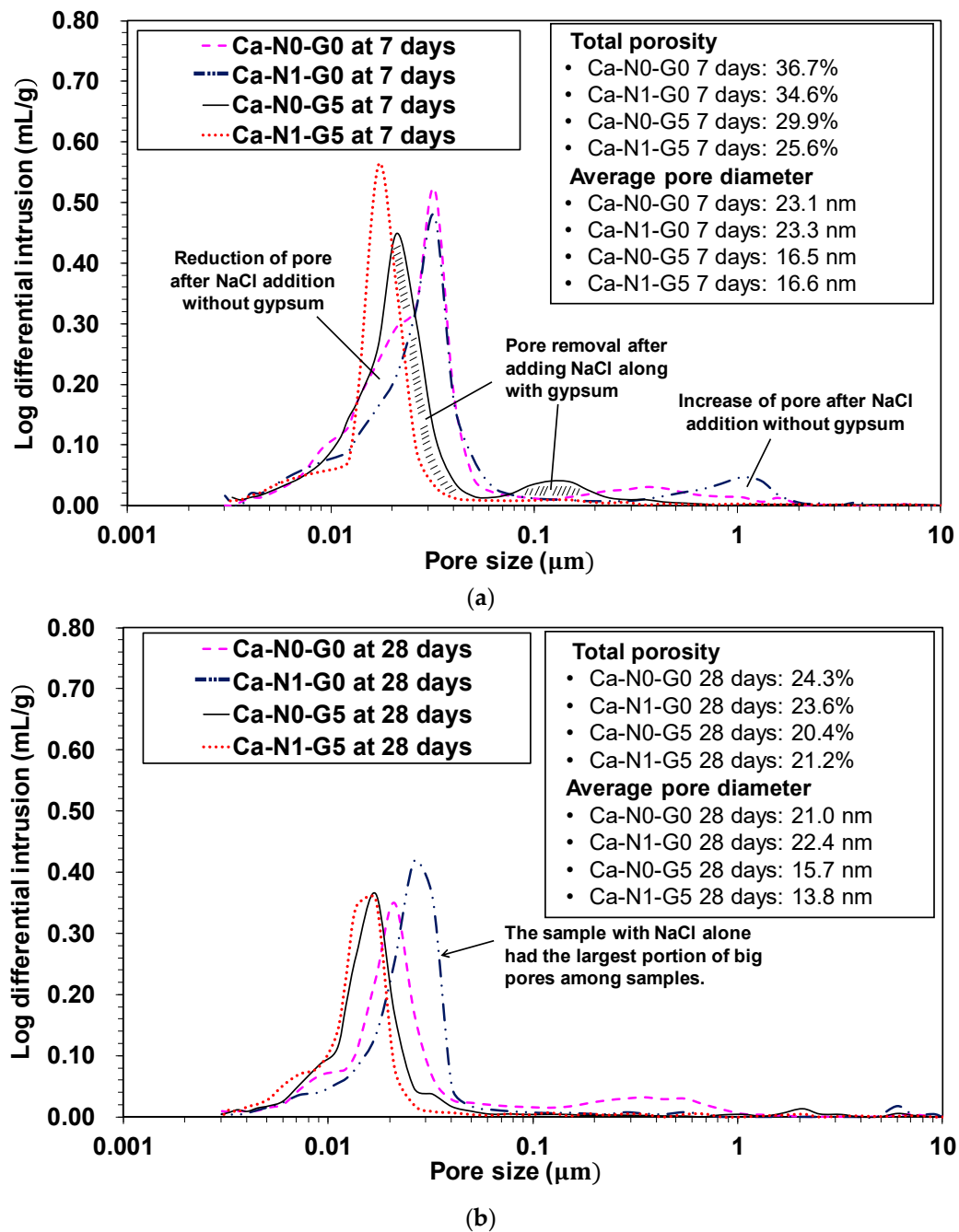
Total porosity
- Ca-N0-G0 7 days: 36.7%
- Ca-N1-G0 7 days: 34.6%
- Ca-N0-G5 7 days: 29.9%
- Ca-N1-G5 7 days: 25.6%

Average pore diameter
- Ca-N0-G0 7 days: 23.1 nm
- Ca-N1-G0 7 days: 23.3 nm
- Ca-N0-G5 7 days: 16.5 nm
- Ca-N1-G5 7 days: 16.6 nm

(**a**)

Total porosity
- Ca-N0-G0 28 days: 24.3%
- Ca-N1-G0 28 days: 23.6%
- Ca-N0-G5 28 days: 20.4%
- Ca-N1-G5 28 days: 21.2%

Average pore diameter
- Ca-N0-G0 28 days: 21.0 nm
- Ca-N1-G0 28 days: 22.4 nm
- Ca-N0-G5 28 days: 15.7 nm
- Ca-N1-G5 28 days: 13.8 nm

(**b**)

Figure 5. Mercury intrusion porosimetry (MIP) results of hardened paste samples at (**a**) 7 days and (**b**) 28 days.

4. Conclusions

This study investigated the influence of adding NaCl to a CaO-activated GGBFS system on strength development, and its dependence on strength enhancement effects on the presence of gypsum in the system. When gypsum was not present, adding NaCl exhibited either no effect or a negative effect on increasing compressive strength, while introducing the inclusion of gypsum used with NaCl allowed NaCl to observably increase the strength, particularly in early days of curing (i.e., before 7 days). The most significant contributor to this strength improvement was likely the increased solubility of gypsum and $Ca(OH)_2$ due to the presence of NaCl in a fresh mixture paste, leading to the more efficient formation of ettringite accompanied by strength improvement in early days of curing. Our conclusions are as follows:

1. Considering that most strength gains of samples with gypsum were obtained by 7 days and the 7-day strength of Ca-N1-G5 was approximately 22% higher than that of Ca-N0-G5, the combined effect of NaCl with gypsum on strength seems to have mostly occurred before three days.

2. In XRD and TG testing, the use of NaCl alone notably formed hydrocalumite, while the incorporation of only gypsum clearly produced ettringite. When NaCl and gypsum were used together, hydrocalumite and ettringite were simultaneously formed; however, no other type of new reaction product was identified.

3. In TG/DTG testing, the use of NaCl likely boosted the formation of ettringite by notably increasing the concentration of sulfate and calcium ions in early days (i.e., before 7 days), resulting in the improvement of strength early in the process.

4. In MIP testing, the use of NaCl did not yield a beneficial influence on pore size distribution for strength improvement at either 7 or 28 days when no gypsum was present. Rather, the use of NaCl hindered pore size refinement from 7 to 28 days. These observations are fairly consistent with their corresponding strength results. However, when gypsum was present, the use of NaCl yielded a significantly advantageous influence on pore size distribution; in particular, at 7 days, the addition of NaCl had removed relatively large pores, possibly due to the increased formation of ettringite.

References

1. Bellmann, F.; Stark, J. Activation of blast furnace slag by a new method. *Cem. Concr. Res.* **2009**, *39*, 644–650. [CrossRef]

2. Gu, K.; Jin, F.; Al-Tabbaa, A.; Shi, B. Activation of ground granulated blast furnace slag by using calcined dolomite. *Constr. Build. Mater.* **2014**, *68*, 252–258. [CrossRef]

3. Shi, C.; Day, R.L. Chemical Activation of Lime-Slag Blends. *Spec. Publ.* **1995**, *153*, 1165–1178.

4. Qing, Y.; Huxing, C.; Yuqing, W.; Shangxian, W.; Zonghan, L. Effect of MgO and gypsum content on long-term expansion of low heat Portland slag cement with slight expansion. *Cem. Concr. Compos.* **2004**, *26*, 331–337. [CrossRef]

5. Wang, S.-D.; Scrivener, K.L. Hydration products of alkali activated slag cement. *Cem. Concr. Res.* **1995**, *25*, 561–571. [CrossRef]

6. Kim, M.S.; Jun, Y.; Lee, C.; Oh, J.E. Use of CaO as an activator for producing a price-competitive non-cement structural binder using ground granulated blast furnace slag. *Cem. Concr. Res.* **2013**, *54*, 208–214. [CrossRef]

7. Taylor, H.F. *Cement Chemistry*; Thomas Telford: London, UK, 1997.

8. Metha, K.; Monteiro, P. *Concrete: Microstructure, Properties, and Materials*, 3rd ed.; McGraw-Hill Publishing: New York, NY, USA, 2006.

9. Wang, S.-D.; Scrivener, K.L.; Pratt, P. Factors affecting the strength of alkali-activated slag. *Cem. Concr. Res.* **1994**, *24*, 1033–1043. [CrossRef]

10. Brough, A.; Holloway, M.; Sykes, J.; Atkinson, A. Sodium silicate-based alkali-activated slag mortars: Part II. The retarding effect of additions of sodium chloride or malic acid. *Cem. Concr. Res.* **2000**, *30*, 1375–1379. [CrossRef]

11. Yang, K.-H.; Cho, A.-R.; Song, J.-K.; Nam, S.-H. Hydration products and strength development of calcium hydroxide-based alkali-activated slag mortars. *Constr. Build. Mater.* **2012**, *29*, 410–419. [CrossRef]

12. Park, H.; Jeong, Y.; Jun, Y.; Jeong, J.-H.; Oh, J.E. Strength enhancement and pore-size refinement in clinker-free CaO-activated GGBFS systems through substitution with gypsum. *Cem. Concr. Compos.* **2016**, *68*, 57–65. [CrossRef]

13. Yum, W.S.; Jeong, Y.; Yoon, S.; Jeon, D.; Jun, Y.; Oh, J.E. Effects of CaCl2 on hydration and properties of lime (CaO)-activated slag/fly ash binder. *Cem. Concr. Compos.* **2017**, *84*, 111–123. [CrossRef]

14. Jeong, Y.; Yum, W.S.; Jeon, D.; Oh, J.E. Strength development and microstructural characteristics of barium hydroxide-activated ground granulated blast furnace slag. *Cem. Concr. Compos.* **2017**, *79*, 34–44. [CrossRef]

15. Delagrave, A.; Marchand, J.; Ollivier, J.-P.; Julien, S.; Hazrati, K. Chloride binding capacity of various hydrated cement paste systems. *Adv. Cem. Based Mater.* **1997**, *6*, 28–35. [CrossRef]

16. Yuan, Q.; Shi, C.; De Schutter, G.; Audenaert, K.; Deng, D. Chloride binding of cement-based materials subjected to external chloride environment–a review. *Constr. Build. Mater.* **2009**, *23*, 1–13. [CrossRef]

17. Al-Akhras, N.M. Durability of metakaolin concrete to sulfate attack. *Cem. Concr. Res.* **2006**, *36*, 1727–1734. [CrossRef]

18. Al-Amoudi, O.S.B.; Maslehuddin, M.; Saadi, M.M. Effect of magnesium sulfate and sodium sulfate on the durability performance of plain and blended cements. *ACI Mater. J.* **1995**, *92*, 15–24.

19. Papadakis, V.G. Effect of supplementary cementing materials on concrete resistance against carbonation and chloride ingress. *Cem. Concr. Res.* **2000**, *30*, 291–299. [CrossRef]

20. Al-Dulaijan, S.U.; Maslehuddin, M.; Al-Zahrani, M.; Sharif, A.; Shameem, M.; Ibrahim, M. Sulfate resistance of plain and blended cements exposed to varying concentrations of sodium sulfate. *Cem. Concr. Compos.* **2003**, *25*, 429–437. [CrossRef]

21. Al-Amoudi, O.S.B.; Maslehuddin, M.; Abdul-Al, Y.A. Role of chloride ions on expansion and strength reduction in plain and blended cements in sulfate environments. *Constr. Build. Mater.* **1995**, *9*, 25–33. [CrossRef]

22. Geng, J.; Easterbrook, D.; Li, L.-Y.; Mo, L.-W. The stability of bound chlorides in cement paste with sulfate attack. *Cem. Concr. Res.* **2015**, *68*, 211–222. [CrossRef]

23. Sotiriadis, K.; Nikolopoulou, E.; Tsivilis, S. Sulfate resistance of limestone cement concrete exposed to combined chloride and sulfate environment at low temperature. *Cem. Concr. Compos.* **2012**, *34*, 903–910. [CrossRef]

24. Madgin, W.; Swales, D. Solubilities in the system $CaSO_4$-NaCl-H_2O at 25° and 35°. *J. Chem. Technol. Biotechnol.* **1956**, *6*, 482–487. [CrossRef]

25. Johnston, J.; Grove, C. The solubility of calcium hydroxide in aqueous salt solutions. *J. Am. Chem. Soc.* **1931**, *53*, 3976–3991. [CrossRef]

26. American Society for Testing Materials. *Standard Test Method for Compressive Strength of Hydraulic Cement Mortars (Using 2-in. or [50-mm] Cube Specimens)*; ASTM C109/C109M-13; ASTM International: West Conshohocken, PA, USA, 2013.

27. Olson, R.A.; Neubauer, C.M.; Jennings, H.M. Damage to the pore structure of hardened Portland cement paste by mercury intrusion. *J. Am. Ceram. Soc.* **1997**, *80*, 2454–2458. [CrossRef]

28. Diamond, S. Mercury porosimetry: An inappropriate method for the measurement of pore size distributions in cement-based materials. *Cem. Concr. Res.* **2000**, *30*, 1517–1525. [CrossRef]

29. Gallé, C. Effect of drying on cement-based materials pore structure as identified by mercury intrusion porosimetry: A comparative study between oven-, vacuum-, and freeze-drying. *Cem. Concr. Res.* **2001**, *31*, 1467–1477. [CrossRef]

30. Morandeau, A.; Thiéry, M.; Dangla, P. Impact of accelerated carbonation on OPC cement paste blended with fly ash. *Cem. Concr. Res.* **2015**, *67*, 226–236. [CrossRef]

31. Gallé, C. Reply to the discussion by S. Diamond of the paper "Effect of drying on cement-based materials pore structure as identified by mercury intrusion porosimetry: A comparative study between oven-, vacuum- and freeze-drying". *Cem. Concr. Res.* **2003**, *33*, 171–172. [CrossRef]

32. Neter, J.; Kutner, M.H.; Nachtsheim, C.J.; Wasserman, W. *Applied Linear Statistical Models*; Irwin: Chicago, IL, USA, 1996; Volume 4.

33. PANalytical, B. *X'Pert HighScore Plus Software*; Version 3.0 e; PANanalytical: Almelo, The Netherlands, 2012.

34. Allmann, R.; Hinek, R. The introduction of structure types into the Inorganic Crystal Structure Database ICSD. *Acta Crystallogr. Sect. A Found. Crystallogr.* **2007**, *63*, 412–417. [CrossRef]

35. Mohan, K.; Taylor, H. Analytical Electron Microscopy of Cement Pastes: IV, β-Dicalcium Silicate Pastes. *J. Am. Ceram. Soc.* **1981**, *64*, 717–719. [CrossRef]

36. Ke, X.; Bernal, S.A.; Provis, J.L. Uptake of chloride and carbonate by Mg-Al and Ca-Al layered double hydroxides in simulated pore solutions of alkali-activated slag cement. *Cem. Concr. Res.* **2017**, *100*, 1–13. [CrossRef]

37. Gruskovnjak, A.; Lothenbach, B.; Winnefeld, F.; Figi, R.; Ko, S.-C.; Adler, M.; Mäder, U. Hydration mechanisms of super sulphated slag cement. *Cem. Concr. Res.* **2008**, *38*, 983–992. [CrossRef]

38. Andrejkovičová, S.; Alves, C.; Velosa, A.; Rocha, F. Bentonite as a natural additive for lime and lime–metakaolin mortars used for restoration of adobe buildings. *Cem. Concr. Compos.* **2015**, *60*, 99–110. [CrossRef]

39. Jun, Y.; Yoon, S.; Oh, J.E. A Comparison Study for Chloride-Binding Capacity between Alkali-Activated Fly Ash and Slag in the Use of Seawater. *Appl. Sci.* **2017**, *7*, 971. [CrossRef]

40. Jeon, D.; Yum, W.S.; Jeong, Y.; Oh, J.E. Properties of quicklime (CaO)-activated Class F fly ash with the use of $CaCl_2$. *Cem. Concr. Res.* **2018**, *11*, 147–156. [CrossRef]

41. Michel, M.; Georgin, J.-F.; Ambroise, J.; Péra, J. The influence of gypsum ratio on the mechanical performance of slag cement accelerated by calcium sulfoaluminate cement. *Constr. Build. Mater.* **2011**, *25*, 1298–1304. [CrossRef]

42. Neto, A.A.M.; Cincotto, M.A.; Repette, W. Mechanical properties, drying and autogenous shrinkage of blast furnace slag activated with hydrated lime and gypsum. *Cem. Concr. Compos.* **2010**, *32*, 312–318. [CrossRef]

43. Shi, C.; Day, R.L. Chemical activation of blended cements made with lime and natural pozzolans. *Cem. Concr. Res.* **1993**, *23*, 1389–1396. [CrossRef]

44. Khan, M.; Kayali, O.; Troitzsch, U. Chloride binding capacity of hydrotalcite and the competition with carbonates in ground granulated blast furnace slag concrete. *Mater. Struct.* **2016**, *49*, 4609–4619. [CrossRef]

45. Bejoy, N. Hydrotalcite. *Resonance* **2001**, *6*, 57–61. [CrossRef]

46. Kayali, O.; Khan, M.; Ahmed, M.S. The role of hydrotalcite in chloride binding and corrosion protection in concretes with ground granulated blast furnace slag. *Cem. Concr. Compos.* **2012**, *34*, 936–945. [CrossRef]

47. Glasser, F.; Kindness, A.; Stronach, S. Stability and solubility relationships in AFm phases: Part I. Chloride, sulfate and hydroxide. *Cem. Concr. Res.* **1999**, *29*, 861–866. [CrossRef]

48. Zhang, L.; Glasser, F. Critical examination of drying damage to cement pastes. *Adv. Cem. Res.* **2000**, *12*, 79–88. [CrossRef]

49. Galan, I.; Beltagui, H.; García-Maté, M.; Glasser, F.P.; Imbabi, M.S. Impact of drying on pore structures in ettringite-rich cements. *Cem. Concr. Res.* **2016**, *84*, 85–94. [CrossRef]

50. Zhou, Q.; Glasser, F.P. Thermal stability and decomposition mechanisms of ettringite at <120 °C. *Cem. Concr. Res.* **2001**, *31*, 1333–1339.

51. Bakolas, A.; Aggelakopoulou, E.; Moropoulou, A.; Anagnostopoulou, S. Evaluation of pozzolanic activity and physicomechanical characteristics in metakaolin-lime pastes. *J. Therm. Anal. Calorim.* **2006**, *84*, 157–163. [CrossRef]

52. Sha, W.; Pereira, G. Differential scanning calorimetry study of hydrated ground granulated blast-furnace slag. *Cem. Concr. Res.* **2001**, *31*, 327–329. [CrossRef]

53. Song, H.; Jeong, Y.; Bae, S.; Jun, Y.; Yoon, S.; Eun Oh, J. A study of thermal decomposition of phases in cementitious systems using HT-XRD and TG. *Constr. Build. Mater.* **2018**, *169*, 648–661. [CrossRef]

54. Vieille, L.; Rousselot, I.; Leroux, F.; Besse, J.-P.; Taviot-Guého, C. Hydrocalumite and its polymer derivatives. 1. Reversible thermal behavior of Friedel's salt: A direct observation by means of high-temperature in situ powder X-ray diffraction. *Chem. Mater.* **2003**, *15*, 4361–4368. [CrossRef]

55. Wei, Y.; Yao, W.; Xing, X.; Wu, M. Quantitative evaluation of hydrated cement modified by silica fume using QXRD, 27 Al MAS NMR, TG–DSC and selective dissolution techniques. *Constr. Build. Mater.* **2012**, *36*, 925–932. [CrossRef]

56. Singh, M.; Garg, M. Calcium sulfate hemihydrate activated low heat sulfate resistant cement. *Constr. Build. Mater.* **2002**, *16*, 181–186. [CrossRef]

57. Glasser, F.; Pedersen, J.; Goldthorpe, K.; Atkins, M. Solubility reactions of cement components with NaCl solutions: I. $Ca(OH)_2$ and CSH. *Adv. Cem. Res.* **2005**, *17*, 57–64. [CrossRef]

58. Nyame, B.; Illston, J. Capillary pore structure and permeability of hardened cement paste. In Proceedings of the 7th International Congress on the Chemistry of Cement, Paris, France, 30 June–4 July 1980.

59. Kendall, K.; Howard, A.; Birchall, J.D. The relation between porosity, microstructure and strength, and the approach to advanced cement-based materials. *Philos. Trans. R. Soc. Lond. A* **1983**, *310*, 139–153. [CrossRef]

60. Luping, T. A study of the quantitative relationship between strength and pore-size distribution of porous materials. *Cem. Concr. Res.* **1986**, *16*, 87–96. [CrossRef]